Dynamic response of a reinforced concrete slab subjected to air blast load

Y.S. Tai [a,*], T.L. Chu [b], H.T. Hu [c], J.Y. Wu [c]

[a] Department of Civil Engineering, ROC Military Academy, 1 Wei-Wu Rd, Feng-Shan 830, Taiwan, ROC
[b] Institute of Nuclear Energy Research, Atomic Energy Council, Taiwan, ROC
[c] Department of Civil Engineering, National Cheng Kung University, Taiwan, ROC

ARTICLE INFO

ABSTRACT

Reinforced concrete is the principal material for military engineering and nuclear power plant containment. However, impacts and explosions could completely destroy such structures, causing tremendous casualties and property loss. Hence, this study conducts an analysis on the propagation law of a blast pressure wave and the dynamic response of reinforced concrete structures under explosive pressure wave effects. This study uses proper state material parameters and equations and then applies the nonlinear finite element analysis software LS-DYNA to conduct a numerical simulation of a free-field explosion model. After comparison with the computed results from empirical equations and validating the reliability of the numerical analysis model, the destruction and influencing factors on reinforced concrete slabs, under the effects of a blast pressure wave, are investigated. The results can serve as a reference for future analysis and design.

© 2011 Elsevier Ltd. All rights reserved.

1. Introduction

Reinforced concrete is the principal material used for the military engineering and containment of nuclear power plants. Its mechanical responses under the effects of dynamic loads are complicated. If the load acts slowly on a large plane, it can be analyzed using the structural mechanics theory. If the load acts rapidly on the concrete structure, due to the inertia and a short duration effects, the response forms a local region of high pressure and high temperature. The response is centered on the load point and an outgoing shock wave is formed inside the concrete. The compressive wave reflection from the rear faces of the target produce a tensile wave which interacts with compressive waves resulting in spalling. Concrete behavior is also different from that under the effect of a quasi-static load. This problem is complicated as the behavior of the material is difficult to control and the mechanical behaviors vary under different load conditions. The methods for studying this problem include (1) analytical methods: under appropriate assumed conditions, solving the problem using a theoretical model after idealizing the shock wave propagation or impact load, however this method is only applicable to simple problems; (2) experiments: conducting small-scale or prototype testing experiments by selecting the proper effect parameters for the blast pressure wave and analyzing the results using the statistical regression method to obtain the empirical formula or figures for the structural dynamic response; (3)

numerical analysis: using a computer and the fundamental laws of mechanics (the laws of mass, energy, and momentum), to properly introduce a dynamic response in the material and the failure criterion using numerical methods, such as the finite element method or finite difference method [1–6].

A number of papers [7–10] conducted in-depth studies on the propagation law of blast pressure waves in different mediums and proposed some computing formulas. The work in [11] proposed the equivalent conversion law for different kinds of explosives. The TM5-855-1 [12] and TM5-1300 [13] explained the principles of explosion and calculation methods. To explore the anti-explosion performance of structural components, [14] carried out experiments and numerical simulations on the visco-plastic behavior of thin metallic plates subjected to an explosion. The work in [15] conducted experimental and numerical studies on the response of stiffened slabs subjected to gas explosions. The work in [16] analyzed the transient response of isotropic and laminated plates to close proximity blast loads. Li et al. [17] investigated the explosion resistance of a metallic plate with a square hole. The work in [18] studied the modeling considerations of impulsive loads on reinforced concrete slabs. Hao et al. [19] conducted numerical analysis on the elastic–plastic dynamic response of steel columns subjected to the pressure wave from an underground explosion. In [20] performed an analysis on explosive damage to reinforced concrete columns. In respect to the explosion resistance of walls, Nash et al. [21] examined the spall damage to concrete walls from close-up cased and uncased explosions in the air. Varma et al. [22] discussed the damage to brick masonry

* Corresponding author.
  E-mail address: ystai@cc.cma.edu.tw (Y.S. Tai).

panel walls under high explosive detonations. Makovicka [23] studied the dynamic response of thin masonry walls under explosion effects. Mays et al. [24] considered the dynamic response to the blast load of concrete wall panels with openings.

Although the above studies provided plentiful results, considering the dynamic response of reinforced concrete structures subjected to blast loads is complicated, this study conducts an analysis of the dynamic response and damage pattern of an RC plate subjected to different blast loads using the nonlinear finite element analysis program LS-DYNA [25]. The results can serve as reference for future analysis and design.

2. Law of propagation of explosions in the air

The sudden release of energy from an explosion in the air produces an instantaneous high-temperature, high-pressure detonation wave in the atmosphere. This pressure wave causes the rapid expansion and propagation of ambient gases. The high-pressure air at the front end of these gases contains most of the explosive energy and is known as the blast pressure wave. The energy carried by the blast pressure wave will decrease as the propagation distance and time increases. The pressure behind the shock wave front can instantly reduce to below the air pressure of the surrounding atmosphere. During the negative pressure phase, the air is evacuated to create a vacuum and the pressure and temperature then return to the same as that of the ambient air. A typical explosion pressure time history curve is shown in Fig. 1. Before the arrival of the shock wave, the atmospheric pressure is P_0; at t_A. After the explosion, the pressure abruptly rises to overpressure peak P_{s0}, then attenuates to P_0 at $t_A + t_0$, later arriving at the negative pressure peak P'_{s0}, and finally returning to P_0 at $t_A + t_0 + t'_0$. Due to the complexity of the explosion process, it is difficult to obtain the parameters of the blast pressure wave through theoretical analysis. Baker [8] proposed an equation to express the pressure attenuation process and controlled it using attenuation factor α:

$$P_{s0}(t) = P_{s0}\left(1 - \frac{t}{t_0}\right)e^{\frac{-\alpha t}{t_0}} \tag{1}$$

where t is the pressure wave duration time. The impulse formed by positive pressure can be obtained using its integral to time.

$$i_{so} = \int_{t_A}^{t_A+t_0} P_{s0}(t)dt \tag{2}$$

Some studies have summarized several usable empirical equations for shock wave parameter calculation through theoretical analysis and numerous experimental studies. The commonly used empirical equations include that proposed by [26]:
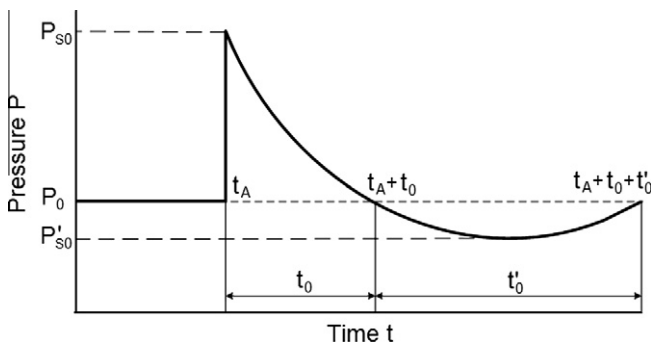
$$P_{s0} = 1.4072Z^{-1} + 0.554Z^{-2} - 0.0357Z^{-3} + 0.000625Z^{-4}(0.1 \leqslant Z \leqslant 0.3)$$
$$P_{s0} = 0.619Z^{-1} - 0.033Z^{-2} + 0.213Z^{-3}(0.3 \leqslant Z \leqslant 1)$$
$$P_{s0} = 0.066Z^{-1} + 0.405Z^{-2} + 0.329Z^{-3}(1 \leqslant Z \leqslant 10)$$
$$\tag{3}$$

Baker's equation [8]:

$$P_{s0} = 20.06Z^{-1} + 1.94Z^{-2} - 0.04Z^{-3}(0.05 \leqslant Z \leqslant 0.5)$$
$$P_{s0} = 0.67Z^{-1} + 3.01Z^{-2} + 4.31Z^{-3}(0.5 \leqslant Z \leqslant 70.9)$$
$$\tag{4}$$

and Brode's equation [27]:

$$P_{s0} = \frac{0.975}{Z} + \frac{1.455}{Z^2} + \frac{5.85}{Z^3} - 0.019 \quad 0.1 < P_{s0} < 10bar$$
$$P_{s0} = \frac{6.7}{Z^3} + 1 \quad P_{s0} > 10bar$$
$$\tag{5}$$

where Z is the scaled distance, expressed by $Z = R/W^{1/3}$.

3. Analysis of reinforced concrete plate subjected to a blast pressure wave

In the analysis model built upon Lagrangian elements for explosives and ambient mediums, the finite element mesh instantly distorts when studying the blast pressure wave effects on the structure and the medium moving with the explosives. Hence, the Jacobian of the integration point may become a negative value and the stable time step size needed for the calculation approaches zero. As a result, either the overall computing time extends infinitely or the computing process diverges. If the model is built using Eulerian elements and the mesh remains unmoved, numerous Eulerian elements are required to trace the dynamic response of the structures, which may cause errors due to the computation of complex changes to the interface. Therefore, this study applied the ALE method, which integrates the advantages of the Lagrangian and Eulerian elements but without the excessive mesh distortion problem, to the proposed method effectively traces the movement of structural boundaries and observes the blast pressure wave's pressure distribution in the medium while the blast load is occurring. The analysis model and the definition of materials are detailed as follows.

3.1. Analysis model

The geometry of the reinforced concrete slab is shown in Fig. 2, where the length is 3.6 m, the width 3.0 m, and the thickness 0.15 m. There were 18 steel bars in the x direction and 15 in the y direction. The explosives were placed 2.5 m above the center of the model. The structure and load were symmetrical, so half of the model was taken for analysis in order to simplify the computing. The finite element model is shown in Fig. 3. During the computing process, the explicit time integration method was employed to compute the time integration. Since it is a conditional stable integration method and the integration time step size is a function of the characteristic mesh length. Accordingly, a time step scale factor of 0.6 is defined to ensure convergence. However, for the air mesh division, apart from the integration stability, the shock wave period must be considered as it may refract or reflect and thus lead to energy decay if the shock wave meets gaps or boundaries while propagating in the medium. To avoid this phenomenon during the computation as well as errors in the analysis, the shock wave for every time step should not exceed the size of two elements. The shock wave wavelength is in direct proportion to the shock wave period, so the minimum element length is determined by the shock wave duration, generally $L_{max} < cT/n$, where c is the sound velocity of the medium and n is the wavelength of the shock wave within the elements. This research used $n = 9$, so the length of the air mesh was 100 mm.
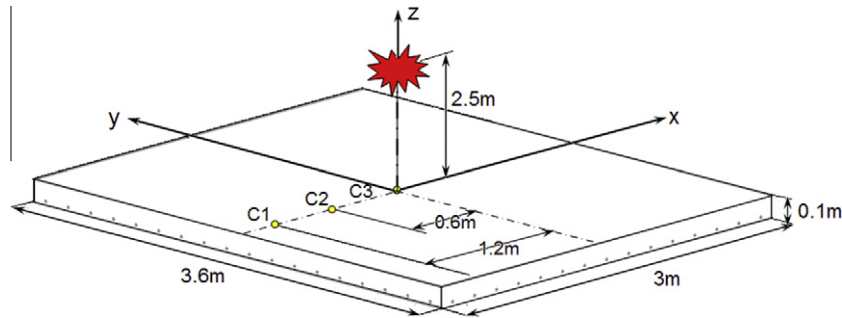

Fig. 1. Typical pressure time history for air blast.

Fig. 2. The geometric configuration of the reinforced concrete slab.
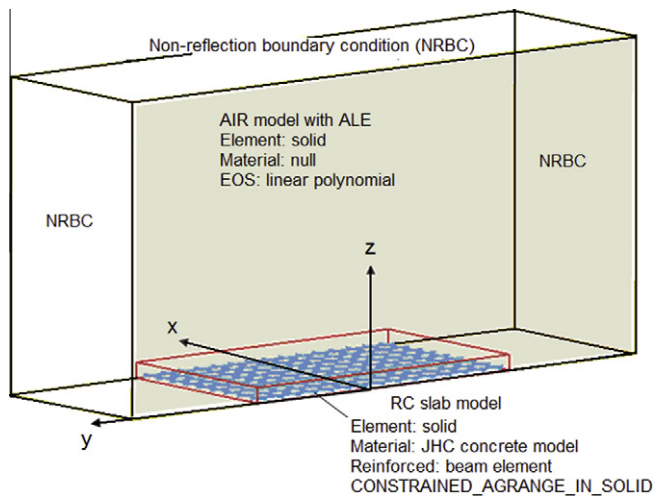

Fig. 3. Finite element model.

3.2. Boundary condition

Considering the boundary condition, protective structures are divided into numerous small slabs stiffened primarily by beams. The edges of these slabs can provide restraint at the moment due to the torsion rigidity of the beams. Therefore the four sides of the reinforced concrete slab have clamped boundaries during analysis. The boundary of the air medium may make the shock wave refract or reflect, so that it superposes or is canceled out by the incident waves in the analysis domain. To avoid this problem, the boundary condition around the air medium is set as a non-reflecting boundary, thus the pressure would flow out at this boundary and not cause reflection.

In the nonlinear finite element analysis of reinforced concrete, reinforced effect simulation utilizes three methods: separation mode, combination mode and entirety mode. If the local damage to the reinforced concrete is subjected to an explosion effect, the separate type is adopted because the composite type and the entirety type have a poor computing accuracy and cannot observe the damage of reinforced steel. Therefore, this study used the separate type model for analysis. Reinforced steel is employed in the beam element and the concrete utilized the hexahedron continuum elements for simulation. The bonding of reinforced steel and concrete coupled the reinforced steel element and concrete element through the CONSTRAINED_LAGRANGE_IN_SOLID command. It was supposed that there was a high bond between the reinforced steel and concrete under the instantaneous impulse external force effect without sliding between them.

4. Constitutive laws and the equation of state

4.1. Concrete

The dynamic behavior of concrete determines the concrete's strength characteristics. The constitutive law employs the plastic flow rule on its principal stress space to differentiate between the hydrostatic and deviatoric stress portions. Different load functions are used to describe the behavior of the two parts. The material model based on a low compressive pressure zone is described in terms of the deviatoric stress. In the impacting process where the shock pressure induced on the material interior is at maximum strength, the deviatoric stress portion has a small influence. The material can be regarded as compressible fluid. The Hugoniot shock pressure and specific volume relationship (EOS) is applied to replace the stress–strain relationship. To fully describe the concrete's dynamic effect within the impact procedure, several concrete models have been implemented in LS-DYNA, designed for special purposes such as damage, effect of strain rate and cracks [28–31]. This investigation applies results from the perforation simulations with the LS-DYNA and the "Johnson–Holmsquist Concrete" material model, based on work by Holmquist, Johnson and Cook to forecast material behavior [29,30]. The equivalent strength model, accumulated damage model and EOS are described as follows.

4.1.1. Equivalent strength model

The equivalent strength component of the model is given by

$$\sigma^* = [A(1 - D) + BP^{*N}] \cdot [1 + C \ln \dot{\varepsilon}^*] \qquad (6)$$

The normalized equivalent stress is given by $\sigma^* = \sigma/f_c'$, where σ represents the actual equivalent stress, and f_c' denotes the quasi-static uni-axial compressive strength; P^* denotes the normalized pressure, shown as $P^* = P/f_c'$; $\dot{\varepsilon}^*$ denotes the dimensionless strain rate, given by $\dot{\varepsilon}^* = \dot{\varepsilon}/\dot{\varepsilon}_0$; $\dot{\varepsilon}$ represents the actual strain rate; $\dot{\varepsilon}_0 = 1.0s^{-1}$ represents the reference strain rate; $D(0 \leqslant D \leqslant 1)$ denotes the damage parameter and the normalized largest tensile strength is given by $T^* = T/f_c'$, where T represents the maximum tensile stress. Additionally A, B, N, C, and S_{max} denote the material parameters, respectively, as normalized cohesive strength, normalized pressure hardening coefficient, pressure hardening exponent, strain rate coefficient and normalized maximum strength.

4.1.2. Accumulated damage failure model

The accumulated damage failure model for concrete is similar to that in the Johnson Cook fracture model [32]. In addition to the damage accumulated in equivalent plastic stain, the Johnson–Holmquist concrete model also considered owing to the plastic volumetric strain. The damage model is written as

$$D = \sum \frac{\Delta \varepsilon_p + \Delta \mu_p}{\varepsilon_p^f + \mu_p^f} \qquad (7)$$

Here $\Delta \varepsilon_p$ and $\Delta \mu_p$ represent the equivalent plastic strain increment and plastic volumetric strain increment, respectively, during one cycle integral computation. The equation

$$f(P) = \varepsilon_p^f + \mu_p^f = D_1 (P^* + T^*)^{D_2} \qquad (8)$$

represents the plastic strain to fracture under a constant pressure, where D_1 and D_2 represent damage constants.

4.1.3. The equation of state, EOS

The EOS describes the relationship between hydrostatic pressure and volume. The concrete loading and unloading process can be divided into three response regions. The first zone is the linear elastic zone, arising at $P \leqslant P_{crush}$, where the material is in the elastic state. The elastic bulk modulus is given by $k = P_{crush}/\mu_{crush}$, where P_{crush} and μ_{crush} represent the pressure and volumetric strain arising in a uni-axial compression test. Within the elastic zone, the loading and unloading equation of state is given by

$$P = K\mu \qquad (9)$$

where $\mu = \rho/\rho_0 - 1$; ρ denotes the current density, and ρ_0 denotes the reference density. The second zone arises at $P_{crush} < P < P_{lock}$, where the material is in the plastic transition state. In this area, the concrete interior voids gradually reduce in size as the pressure and plastic volumetric strain increase. The unloading curve is solved by the difference from the adjacent regions. The third area defines the relationship for fully dense material. The concrete has no air voids and thus fulfills the condensed material Hugoniot relationship. The pressure and the volumetric strain relationship is given by

$$P = K_1 \bar{\mu} + K_2 \bar{\mu}^2 + K_3 \bar{\mu}^3 \qquad (10)$$

where $\bar{\mu} = \frac{\mu - \mu_{lock}}{1 + \mu_{lock}}$ represents the corrected volumetric strain, and K_1, K_2, K_3 are constants. The tensile pressure is restricted to $T(1 - D)$. To identify each material parameter in the constitutive law, the tri-axial compression and high strain rate dynamic tests must be performed on the concrete samples. This derives the concrete's EOS and material strength parameters. The material parameters in this analysis are shown in Table 1.

4.2. Steel bar

Reinforcing steel bars observe the elasto-plastic constitutive law. The hardened model used was the isotropic hardening rule, which applies the largest plastic strain as its failure threshold. Once the element approaches this plastic strain in the computation procedure the element is regarded as failed and eroded. Moreover,

when the material is subjected to a short-term dynamic load, its stress–strain relationship determines the value of the strain and assumes the change to be inversely proportional. Many investigations have already considered various constitutive laws concerning the strain rate's influence on the material properties. The constitutive law of the material is found when the stress–strain relationship using the regression formula is obtained from the material dynamic load. Nevertheless, to maintain the required material parameters with the constitutive law, a similar test must be conducted every time and a regression analysis performed on the test results. The work in [33] presented a simple equation to obtain the dynamic yield stress from the static strength:

$$\dot{\varepsilon} = D \left(\frac{\sigma_{dy}}{\sigma_y} - 1 \right)^n \quad \sigma_{dy} > \sigma_y \qquad (11)$$

$$\sigma_{dy} = \sigma_y \lfloor 1 + |\dot{\varepsilon}/D|^{1/n} \rfloor \qquad (12)$$

where $\dot{\varepsilon}$ denotes the truth strain rate; σ_{dy} denotes the rate related to the dynamic yield stress; σ_y represents the static yield stress; D and n represent the material parameters. Considering mild steel, in [34] demonstrated when $D = 40\ \mathrm{s}^{-1}$ and $n = 5$, the predicted results and experimental data agree. The reinforcing bar's material parameters are listed in Table 2.

4.3. Material failure

The erosion algorithm is implemented to simulate the crushing of concrete in the numerical model. When the material response in an element reaches a certain critical value, the element is immediately deleted. Fig. 4 shows an example calculation for a concrete plate subjected to blast using the erosion algorithm. The fracture details are revealed from the simulation in a rather realistic manner. There may be a variety of criteria governing the material erosion. Typically, the material fracture and failure under tension and compression may be defined by the magnitude of the effective plastic strain and volumetric tensile strain, respectively. The effective plastic strain is given by

$$\bar{\varepsilon}_p = \int_0^t \left(\frac{2}{3} D_{ij}^p D_{ij}^p \right)^{1/2} dt \qquad (13)$$

where D_{ij}^p denotes the plastic component of the rate of deformation tensor. Typical concrete strain at peak tensile stress under static loading is around one-tenth of that at peak compressive stress. Considering the softening phase, the concrete at fracture with practically complete loss of tensile strength may be assumed as 0.001. For the explosion cases under consideration, the maximum strain rate is generally on the order of 10–100 s^{-1}. For this magnitude of

Table 1
The material parameters for the concrete model.

Density, ρ_0 (kg/m³)	Shear modulus, G (MPa)	Strength constants					
		A	B	N	C	f_c'	S_{max}
2320	8.2×10^3	0.79	1.6	0.61	0.007	17.2	7.0
	T	$\dot{\varepsilon}$					
	1.37	1.0					

D_1							D_2
Damage constants							
0.04							1.0

P_{crush} (MPa)	μ_{crush}	K_1 (GPa)	K_2 (GPa)	K_3 (GPa)	P_{lock} (GPa)	μ_{lock}
Equation of state, EOS constants						
16.0	0.001	85.0	−171.0	208	0.8	0.1

Table 2
The material parameters for the reinforced bar.

Density, ρ_0 (kg/m³)	Yield stress (MPa)	Elastic modulus (GPa)	Poisson's ratio	Maximum plastic strain
7800	414	210	0.3	0.12
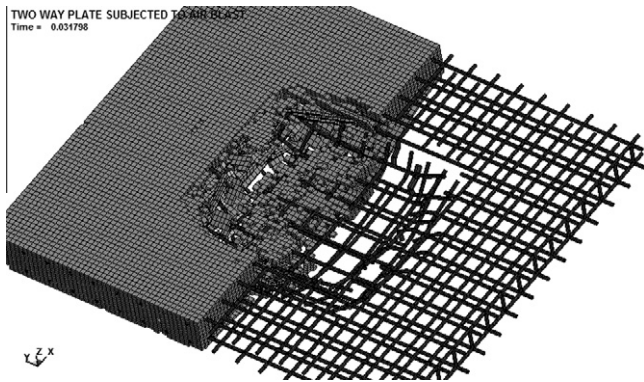
Fig. 4. Typical concrete destruction simulation using the erosion algorithm.

strain rate, the corresponding dynamic strength enhancement factor can reach 5.0 or above. Taking all these influences into account and in conjunction with trial parametric analysis, it is found that the dynamic tensile fracture strain should be around 0.01 for spallation with the RC material. Thus, the principal tensile strain reaching 0.01 is adopted as the primary criterion in erosion algorithm implementation in the numerical simulation.

4.4. Equation of state

4.4.1. Explosive

The pressure released by chemical energy during the explosion is simulated using JWL EOS, and its detonation velocity is 6930 m/s.

$$p = A\left(1 - \frac{\omega\eta}{R_1}\right)e^{-R_1/\eta} + B\left(1 - \frac{\omega\eta}{R_2}\right)e^{-R_2/\eta} + \omega\eta\rho_0 E \quad (14)$$

where A, B are linear explosion coefficients, ω, R_1, R_2 are nonlinear explosion coefficients, $\eta = \rho/\rho_0$, ρ_0 is the initial density of the material and E is the specific internal energy of every unit of mass. When the blasting powders are TNT, according to the explosives manual [35], the aforesaid parameters are respectively $A = 3.712 \times 10^{11}$ Pa, $B = 3.231 \times 10^9$ Pa, $\omega = 0.30$, $R_1 = 4.15$, $R_2 = 0.95$, $\rho_0 = 1630$ kg/m³, $E = 4.29 \times 10^6$ J/kg.

4.4.2. Air

In this study, the LINEAR_POLYNOMIAL equation of state is used to describe the behavior of the air.

$$P = C_0 + C_1\mu + C_2\mu^2 + C_3\mu^3 + (C_4 + C_5\mu + C_6\mu^2)E_0 \quad (15)$$

where E_0 is the initial energy density, and $\mu = \rho/\rho_0 - 1$, $C_i (i = 0\text{–}6)$ are the coefficients. For ideal gases, the coefficients in the EOS are $C_0 = C_1 = C_2 = C_3 = C_6 = 0$, and $C_4 = C_5 = \gamma - 1$. Thus the EOS can be simplified as Gamma Law EOS:

$$P = (\gamma - 1)\frac{\rho}{\rho_0}E_0 \quad (16)$$

where ρ/ρ_0 is the relative density, γ is the rate of change to the specific heat of air, ρ_0 is the initial air density value, and ρ is the current air density. For the initial internal energy, under standard atmospheric pressure, according to the Gamma law calculation, at $\gamma = 1.4$, its initial internal energy is $E = 2.5 \times 10^5$ J/kg.

5. Results and discussion

In order to validate the accuracy of the analysis results, we conducted a free-field explosion simulation and compared the blast pressure wave parameters. Fig. 5 shows a time history comparison of the finite element mesh to blast pressure. When the time history comparison was conducted at a distance of 200 cm from the center point of the explosion, it was found that the blast pressure wave time is very short. The blast pressure wave attenuates quickly after arriving at the peak. As shown in the figure, the blast pressure wave curve, as simulated by this study, indicates the same trend from an ideal blast pressure wave. However, the peak pressure and attenuation differ due to the different mesh densities. The peak pressure is calculated according to the eq. (3), is 15.48 MPa. The numerical result of 13.20 MPa is for 10 cm mesh, 9.0 MPa for 20 cm mesh, and 3.85 MPa for 40 cm mesh, respectively. This indicates that the mesh quality has great influence on the pressure–time history curve. Fig. 6 shows a comparison of the numerical simulation and the peak pressure results according to the Eqs. (3) and (4) under different scaled distance Z, ($Z = R/W^{1/3}$). The 40 cm mesh result is obviously different from the empirical equation results. However, the curve trend for 10 cm and 20 cm meshes is consistent with the empirical equation results.
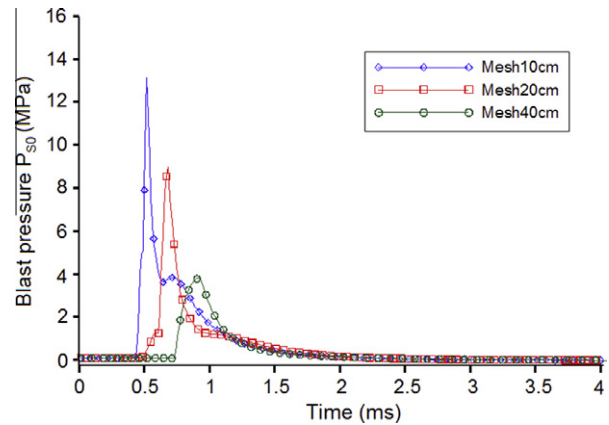
Fig. 5. Time history comparison of finite element mesh to blast pressure.
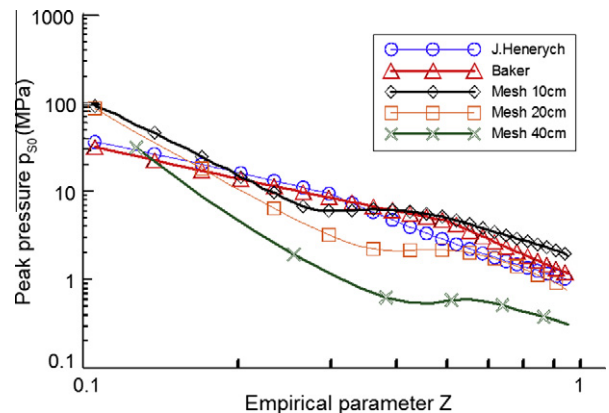
Fig. 6. Comparison of the peak pressure in the numerical simulation and empirical equation.
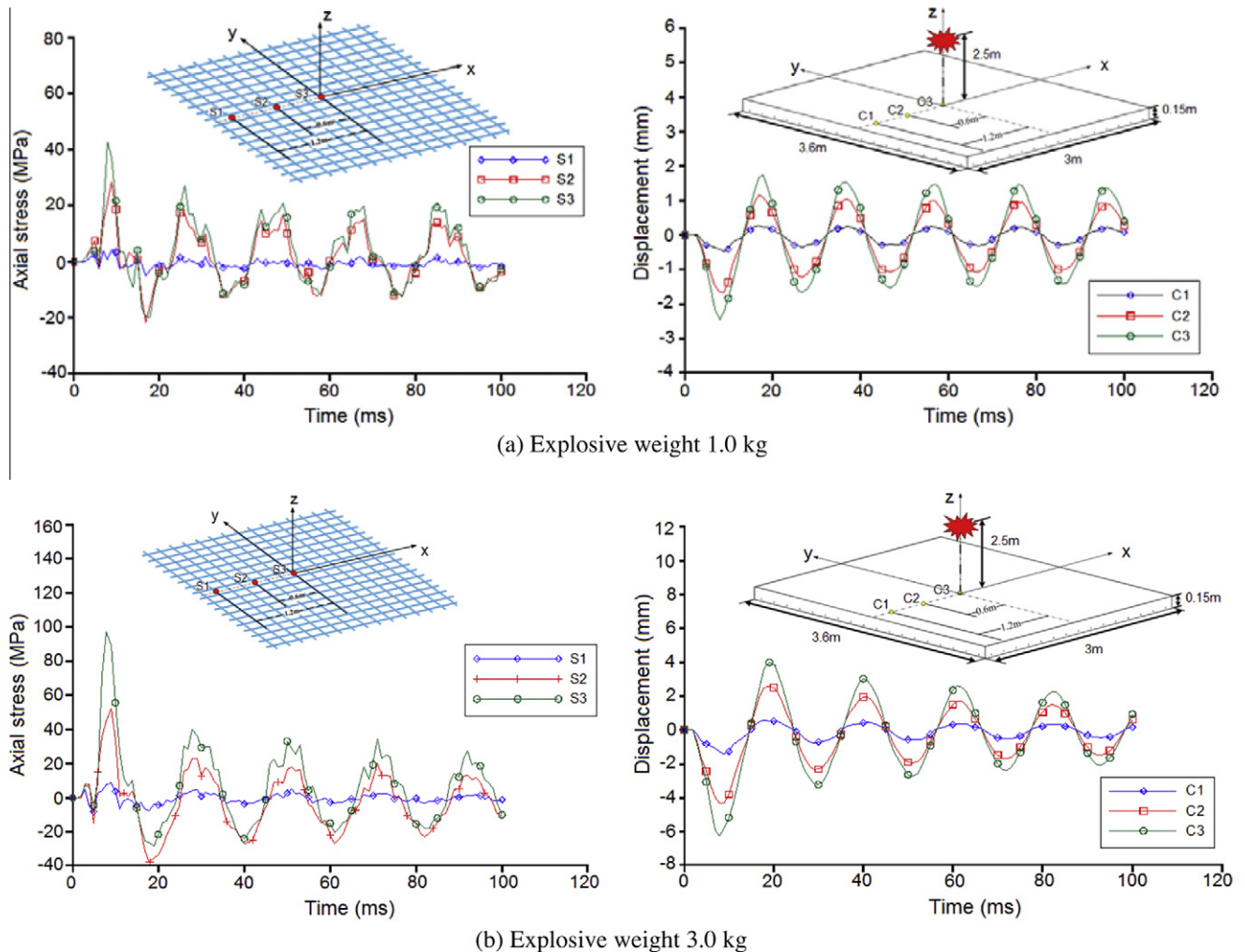
(a) Explosive weight 1.0 kg

(b) Explosive weight 3.0 kg

Fig. 7. Analysis results for reinforcing bar stress and RC slab displacement history.

This study employed the above methods to discuss the destructive effects on an RC slab under the influence of the following factors: different amounts of explosives, different reinforcement ratios and distance from the explosives.

5.1. Effect of explosive amount on the structure

Fig. 7 displays the reinforcing bar's stress and RC slab displacement history analysis results. If the structure is not damaged, 1 kg explosives are the maximum blast load that can be endured by the slab. As shown in Fig. 7a, the blast pressure wave and the effects on the structure reach the maximum value within a very short time. The center point of the reinforced concrete is significantly affected by the explosion. The steel axial stress is 42.6 MPa, which is smaller than the yield stress. Therefore, the reinforced concrete has enough resistance. The center point is the closest to the explosion, thus, it bears a largest portion of the blast load. The maximum displacement is 2.44 mm and the spring back is obvious. When the explosive amount is 3 kg, the reinforced concrete slab develops cracks near the support. This model is defined as a slightly damaged model. In other words, the concrete cracks. However, the elements fail to reach failure strain and are damaged. The reinforced stress is 97 MPa (as shown in Fig. 7b). When the amount of explosive is increased to 5 kg, the reinforced concrete slab cracks and damage begins to show (see Fig. 7c) at the support end, which

is a shear failure. The maximum displacement of the center point is 97.5 mm, and the steel axial stress is 130 MPa. If the amount of explosive is increased to 10 kg, damage to both support end elements is observed, as shown in Fig. 7(d). The center of the reinforced concrete slab also develops cracks.

5.2. The reinforcement ratio effect on the structure

The reinforcement ratio range was taken between 0.2% and 1.2% to investigate the reinforcement ratio effect on the RC slab resistance to a blast load. The maximum slab displacement was analyzed under the effects of 10 kg and 20 kg explosives, with the analysis results presented in Figs. 8 and 9. With the increased reinforcement ratio, the center point of the maximum RC slab displacement can be effectively decreased, allowing it to recover soon after reaching maximum displacement, with only small residual deformation. However, this has a great influence on the amount of damage to the concrete. If large amounts of explosives are added, the scope of concrete damage increases largely. With respect to the damage, if the reinforcement ratio is low, the damage occurs mainly in the center of slab. When the reinforcement ratio increases, damage will occur at the support. In other words, the damage to the RC slab changes from bending damage to shear failure.
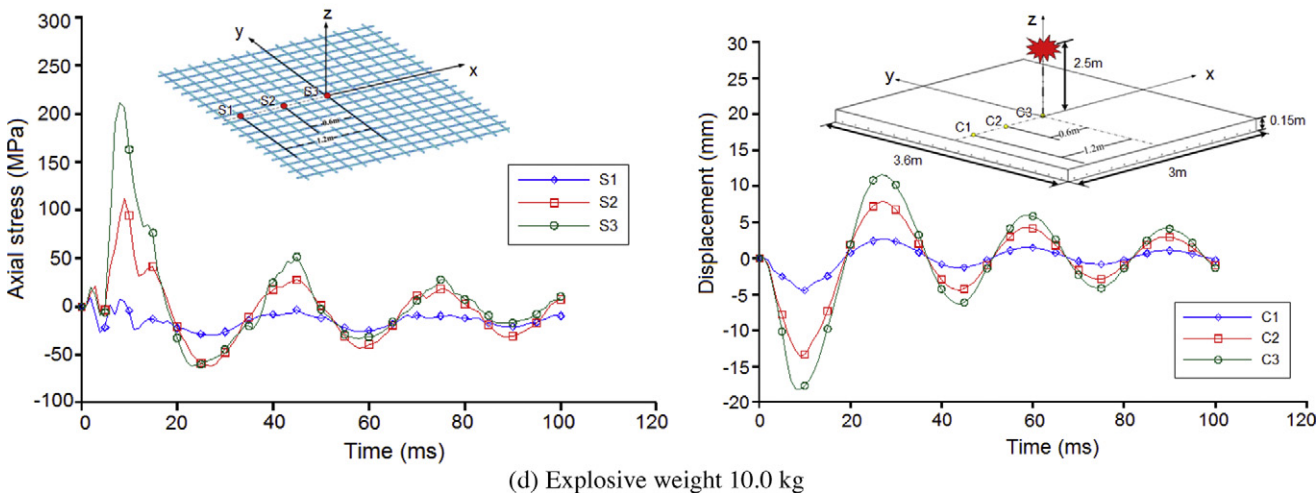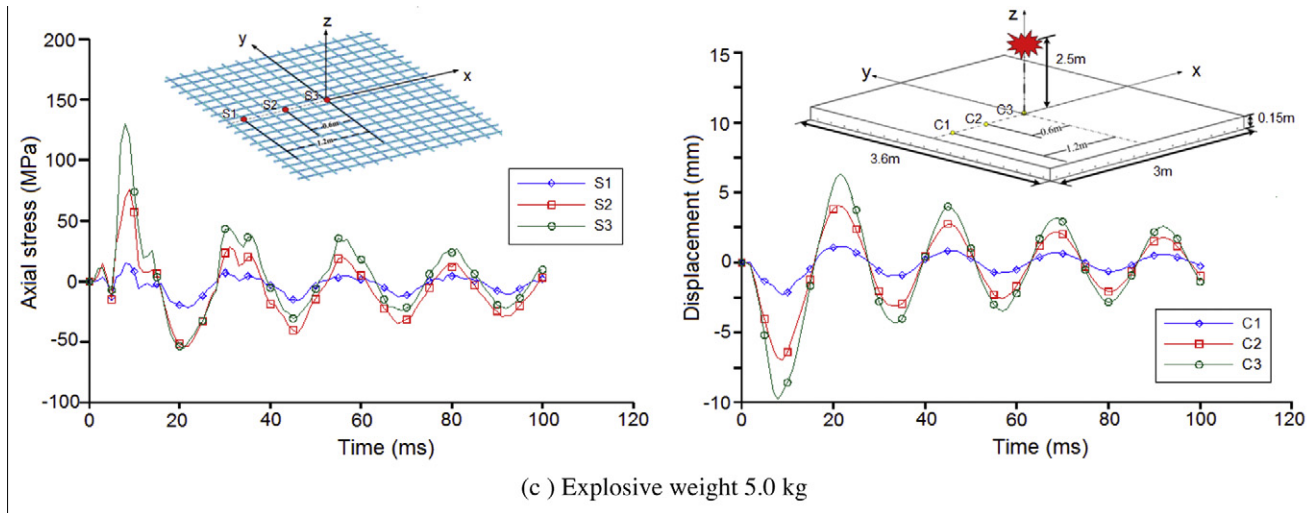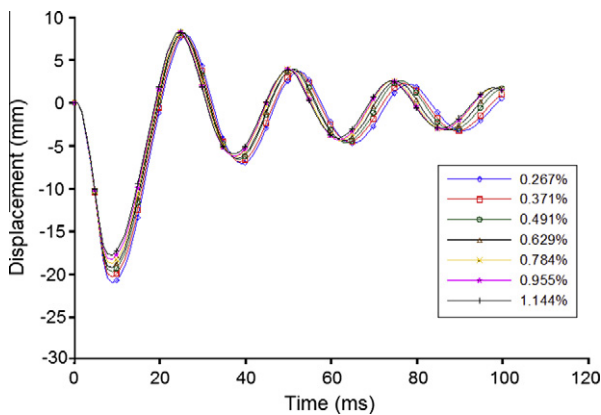
(c) Explosive weight 5.0 kg

(d) Explosive weight 10.0 kg

Fig. 7 (*continued*)

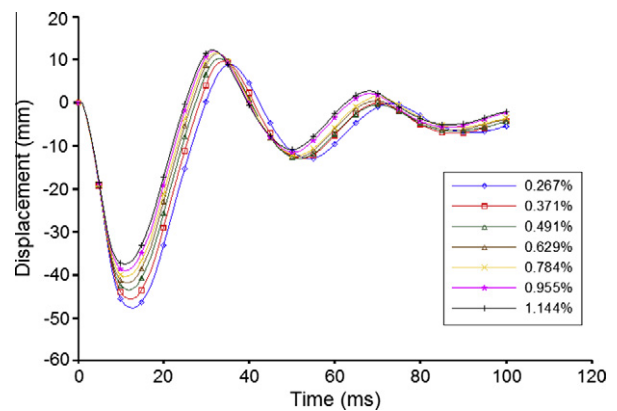**Fig. 8.** The reinforcement ratio effects (explosive weight: 10 kg).

Fig. 9. The reinforcement ratio effects (explosive weight: 20 kg).

5.3. The distance from the explosives effect on the structure

The damage to the reinforced concrete was observed from different distances, from a remote explosion to a short-distance explosion. The distance from the explosion has a significant influence on the slab, which is the same as the blast pressure wave propagation law, as stated in the previous section. If the distance is very short, the Z value of the contraction scale distance is reduced relatively and overpressure is increased relatively. At a distance of 0.5 m, the reinforced concrete slab center is penetrated (as shown in Fig. 10. At a distance of 1.0 m, the reinforced concrete slab center is exploded, creating holes, as shown in Fig. 11.
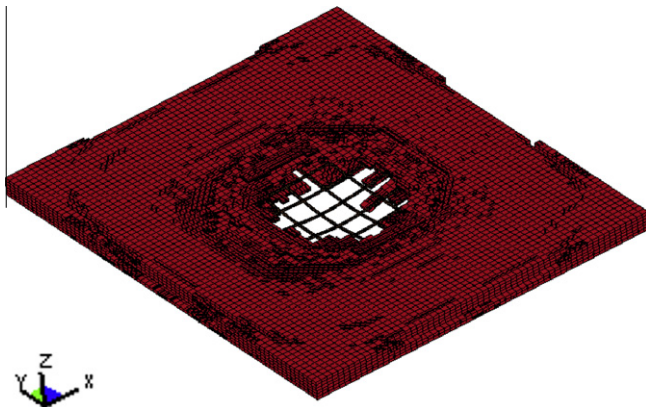
Fig. 10. RC slab damage modes from 10 kg charge and distance 0.5 m case.
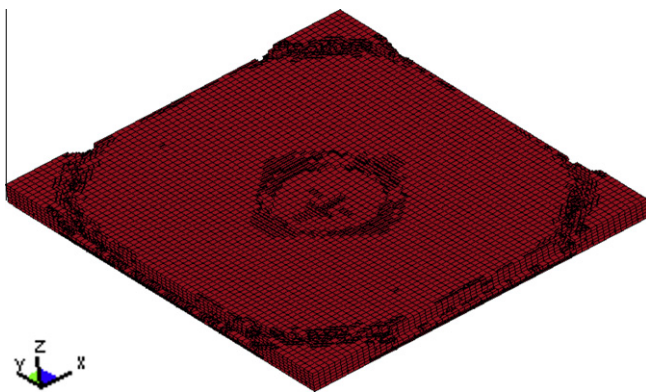

Fig. 11. RC slab damage modes from 10 kg charge and distance 1.0 m.

6. Conclusions

This study employed the nonlinear finite element analysis software LS-DYNA to discuss the dynamic responses of an RC slab under blast load. The results are summarized as follows:

(1) The free-field blast pressure wave simulation indicates that the mesh size is very sensitive to shock wave propagation, thus, to guarantee that the results are close to the actual situation the finite element mesh division should be as fine as possible.

(2) For the RC slab dynamic response the computed results show that under the blast pressure effect, bending damage or shear failure may occur at the center point. The influencing factors include the amount of explosives and distance from the explosives to the RC slab.

(3) If the concrete slab reinforcement ratio is very low the damage may occur at the slab center. However, if the reinforcement ratio is increased the slab deformation is reduced and damage may occur at the support.

References

[1] K. Xu, Y. Lu, Numerical simulation study of spallation in reinforced concrete plates subjected to blast loading, Comput. Struct. 84 (5–6) (2006) 431–438.
[2] J. Leppanen, Concrete subjected to projectile and fragment impacts: modelling of crack softening and strain rate dependency in tension, Int. J. Impact Eng. 32 (2006) 1828–1841.
[3] T. Rabczuk, J. Eibl, Modelling dynamic failure of concrete with meshfree methods, Int. J. Impact Eng. 32 (2006) 1878–1897.
[4] Y. Lu, Modelling of concrete structures subjected to shock and blast loading: an overview and some recent studies, Struct. Eng. Mech. 32 (2) (2009) 235–249.
[5] X.Q. Zhou, V.A. Kuznetsov, H. Hao, J. Waschl, Numerical prediction of concrete slab response to blast loading, Int. J. Impact Eng. 35 (2008) 1186–1200.
[6] S. Gong, Y. Lu, Z. Tu, W. Jin, Validation study on numerical simulation of RC response to close-in blast with a fully coupled model, Struct. Eng. Mech. 32 (2) (2009) 283–300.
[7] G.L. Rogers, Dynamics of Framed Structures, John Wiley & Sons, Inc., New York, 1959.
[8] W.E. Baker, Explosions in Air, University of Texas Press, Austin, TX, 1973. pp. 7–15.
[9] G.F. Kinney, K.J. Graham, Explosive Shocks in Air, Springer-Verlag, New York, USA, 1985.
[10] G.C. Mays, P.D. Smith, Blast Effects on Building, Thomas Telford Publications, London, 1995.
[11] B. Hopkinson. British ordnance minutes 13565, 1915.
[12] TM 5-855-1, Fundamentals of protective design for conventional weapons, Department of the Army, 1986.
[13] TM 5-1300, Structures to resist the effects of accidental explosions, Department of the Army, 1990.
[14] K. Woznica, O. Pennetier, J. Renard, Experiments and numerical simulations on thin metallic plates subjected to an explosion, Journal of Engineering Material and Technology, Transactions of the ASME 123 (2) (2001) 203–209.
[15] Y.G. Pan, L.A. Louca, Experimental and numerical studies on the response of stiffened plates subjected to gas explosions, Journal of Constructional Steel Research 52 (2) (1999) 171–193.
[16] J.M. Coggin, R.K. Kapania, E.R. Johnson, Transient response of laminated plates subjected to close proximity explosions, ASME Aerospace Division AD 58 (1999) 155–162.
[17] G. Li, B.Z. Chen, X.F. Deng, Explosion resistance of a square plate with a square hole, Journal De Physique 12 (7) (2002) 121–124.
[18] N. Duranovic, Impulsive loading on reinforced concrete slabs-modeling considerations, in: International Conference on Structures Under Shock and Impact, SUSI, 1998, pp. 817–826.
[19] H. Hao, H.K. Cheong, S. Cui, Numerical study of dynamic buckling of steel columns subjected to underground explosion, Key Eng Mater 233–236 (2002) 211–216.
[20] R.L. Sheng, E.C. John, B.M. Kenneth, Design of reinforced concrete columns to resist the effects of suitcase bombs, in: The 6th Asia–Pacific Conference Shock and Impact Loads on Structures. Perth W Australia, 2005, pp. 325–331.
[21] P.T. Nash, C.V.G. Vallabhan, T.C. Knight, Spall damage to concrete walls from close-in cased and uncased explosions in air, ACI Struct. J. 92 (6) (1995) 680–688.
[22] R.K. Varma, C.P.S. Tomar, S. Parkash, Damage to brick masonry panel walls under high explosive detonation, 351, Pressure Vessels and Piping Division PVP, ASME, 1997, pp. 207–216.
[23] D. Makovicka, Dynamic response of thin masonry wall under explosion effect, Struct. Mater. 11 (2002) 47–56.
[24] G.C. Mays, J.G. Hetherington, T.A. Rose, Response to blast loading of concrete wall panels with openings, J. Struct. Eng. 125 (12) (1999) 1448–1450.
[25] LS-DYNA, Theoretical Manual, V.971, Livermore Software Technology Corporation, Livermore, CA, USA, 2006.
[26] J. Henrych, The Dynamics of Explosion and its Use, Elsevier Scientific Publishing Company, 1979.
[27] H.L. Brode, Numerical solution of spherical blast waves, J. Appl. Phys. 26 (6) (1955).
[28] L.J. Malvar, J.E. Crawford, J.W. Weswvich, D. Simons, A plasticity concrete material model for dyna3d, Int. J. Impact Eng. 19 (9–10) (1997) 847–873.
[29] T.J. Holmquist, G.R. Johnson, W.H. Cook, A computational constitutive model for concrete subjected to large strains, high strain rates, and high pressures, in: The 14th International Symposium on Ballistics, Quebec City, Canada, 1993, pp. 591–600.
[30] G.R. Johnson, Computed radial stresses in a concrete target penetrated by a steel projectile, in: Proceedings of the 5th International Conference on Structures under shock and impact, Portsmouth, UK, 1998, pp. 793–806.
[31] Z. Tu, Y. Lu, Evaluation of typical concrete material models used in hydrocodes for high dynamic response simulations, Int. J. Impact Eng. 36 (2009) 132–146.
[32] G.R. Johnson, W.H. Cook, Fracture characteristics of three metals subjected to various strains, strain rates, temperatures and pressures, Eng. Fract. Mech. 21 (1985) 31–48.
[33] G.R. Cowper, P.S. Symond, Strain Hardening and Strain Rate Effects in the Impact Loading of Cantilever Beams, Brown University, Division of Applied Mathematics Report, No. 28, 1957.
[34] P.S. Symond, Survey of Methods of Analysis for Plastic Deformation of Structures Under Dynamic Loading, Brown University, Division of Engineering Report, BU/NSRDC/1-67, 1967.
[35] B.M. Dobratz, LLNL Explosive Handbook, UCRL-52997, Lawrence Livermore National Laboratory, Livermore, CA, 1981.